

Research Article

Microstructure and properties of Cu-Al-Ni-Mn-Y alloy with precipitation and effective strengthening by aging treatment

Liu Yang^{a,b,c}, Xiaosong Jiang^{a,b*}, Hongliang Sun^{a,b}, Yali Zhang^d, Yongjian Fang^d, Rui Shu^e

^a*Key Laboratory of Advanced Technologies of Materials, Ministry of Education, Chengdu 610031, China*

^b*School of Materials Science and Engineering, Southwest Jiaotong University, Chengdu Sichuan 610031, China*

^c*Institute for Applied Materials, Karlsruhe Institute of Technology, Engelbert-Arnold-Str. 4, 76131 Karlsruhe, Germany*

^d*School of Mechanical Engineering, Sungkyunkwan University, 2066 Seobu-ro, Jangan-gu, Suwon-si, Gyeonggi-do, 16419, Republic of Korea*

^e*Forschungszentrum Jülich GmbH Institut für Energie-und Klimaforschung Plasmaphysik (IEK-4) 52425 Jülich, Germany*

***Corresponding author:** School of Materials Science and Engineering, Southwest Jiaotong University, Chengdu Sichuan 610031, China.

E-mail: xsjiang@swjtu.edu.cn (**X.S. Jiang**).

Abstract: The Cu-11Al-3Ni-2.5Mn-1Y alloy prepared by hot-press sintering was subjected to aging treatment at different temperatures of 350 °C, 400 °C, 450 °C, 500 °C and 550 °C, respectively. The phase composition, microstructure, mechanical and damping properties were characterized. The results show that the alloys after the ageing treatment are mainly composed of 18R martensite and 2H martensite. The precipitation phase begins to appear and the best comprehensive properties are obtained at the aging temperature of 450 °C. The hardness and strength values reached 347.6 HV and 642.6 MPa, respectively. The strengthening mechanisms are mainly involved in lattice distortion and dislocation increment effect caused by

solution strengthening, shearing and hindering effect of precipitated phases and dislocations, fine grain strengthening effect caused by grain size reduction, and the increase of large angle grain boundary. Simultaneously, the room temperature damping reached 0.0723, which is 93% higher than the original sample of 0.38. The improvement of damping properties is closely related to the changes in the number and size of martensite, the interfacial damping effect caused by precipitated phases, and the pinning and unpinning reaction between dislocations and precipitated phases. Therefore, alloys with both high mechanical and high damping properties can be obtained by proper aging treatment. In addition, the increase in phase transition temperature of high temperature damping properties also provides some guidance for the exploration and development of this alloy in the high temperature field.

Key words: Aging treatment, Microstructure, Precipitated phase, Mechanical properties, Damping properties

1 Introduction

With the development of high-speed and automation in modern industrial machinery, the problems of vibration and noise are becoming more and more serious [1-5]. It can significantly affect the safety of the machinery and endanger the physical and mental health of humans [6-8]. Therefore, it is a very urgent task to develop a damping alloy with high efficiency in consuming mechanical vibrations [9]. Damping alloys such as Ti-Ni [10, 11], Mn-Cu [12, 13], Fe-Mn [14, 15], and Fe-Cr [16, 17] exist defects such as narrow working temperature range, difficult machinability, relatively low damping properties or strong magnetic field dependence. In comparison, the Cu-Al-Ni-Mn alloy has a broad application prospect in the field of vibration reduction due to its stable damping property, excellent thermal stability and relatively simple preparation process [18-24]. However, the inherent large grain structure makes it show relatively poor mechanical properties [25-28]. Generally, the mechanical and damping properties of the material show opposite trends [9, 29, 30]. This becomes the key issue that limits its further development and application. However, in practical engineering applications, alloys with high damping and high mechanical properties

are very necessary. Therefore, it is crucial to find a way that can improve the damping and mechanical properties of Cu-Al-Ni-Mn alloy simultaneously.

In our previous work, the mechanical properties of Cu-Al-Ni-Mn-based alloys were significantly improved by reducing their grain size through alloying [31]. In addition to alloying, heat treatment is considered as another very effective way to enhance the mechanical properties of alloys [2, 3, 18, 32-34]. In recent years, numerous studies have also shown that aging heat treatment can also improve the damping properties by controlling the microstructure [35-38]. Chentouf et al. [39] showed that after aging treatment of Cu-Al-Be alloys, the formation of equilibrium precipitation phase ($\alpha+\gamma_2$) is expected to promote the application of Cu-Al based alloys in more fields. Wang et al. [32] investigated the effect of aging treatment on the microstructure and damping properties of Cu-Al-Mn alloy. The appearance of the precipitated phase and the fineness of the martensite size in the Cu-Al-Mn alloy aged at 350 °C significantly improved the damping properties of the alloy. All these studies indicate that aging can improve the damping and mechanical properties by controlling the precipitation phase. However, the mechanism of the effect of aging precipitation on the damping properties and mechanical properties of Cu-Al-Ni-Mn-based alloys has not been systematically studied.

In this paper, the Cu-11Al-3Ni-2.5Mn-1Y alloy was aged at different temperatures of 350 °C, 400 °C, 450 °C, 500 °C and 550 °C based on previous alloying. Through the characterization and analysis of microstructure, mechanical and damping properties to find out the optimal aging parameters that improve both mechanical properties and damping properties in this experimental range. Furthermore, the strengthening mechanism of aging temperature on the mechanical and damping properties were explored. Meanwhile, it is expected to provide theoretical basis and technical support for expanding the practical applications of Cu-Al based alloys.

2 Experimental processes

2.1 Material preparation

The alloy with nominal composition Cu-11Al-3Ni-2.5Mn-1Y (Wt.%) was prepared from high purity Cu, Al, Ni, Mn and Y powders (purity > 99.5%) by ball milling and vacuum hot-press sintering. Compared to conventional casting, this method shows obvious advantage in preparing high-dense alloys with the homogeneous microstructure and improved properties [40-42]. The density of Cu-11Al-3Ni-2.5Mn-1Y alloy prepared reached $98.6 \pm 0.3\%$, showing relatively low porosity. The specific details of this preparation process can be found in our previous work [31]. Then the prepared alloy was heated to 900 °C in a vacuum heat treatment furnace, and held at this temperature for 60 min before water quenching. Subsequently, the water-quenched samples were held at 350 °C, 400 °C, 450 °C, 500 °C and 550 °C for 30 min and air-cooled to room temperature. The flow chart of sample preparation and heat treatment process parameters are shown in Figure 1 and Table 1, respectively.

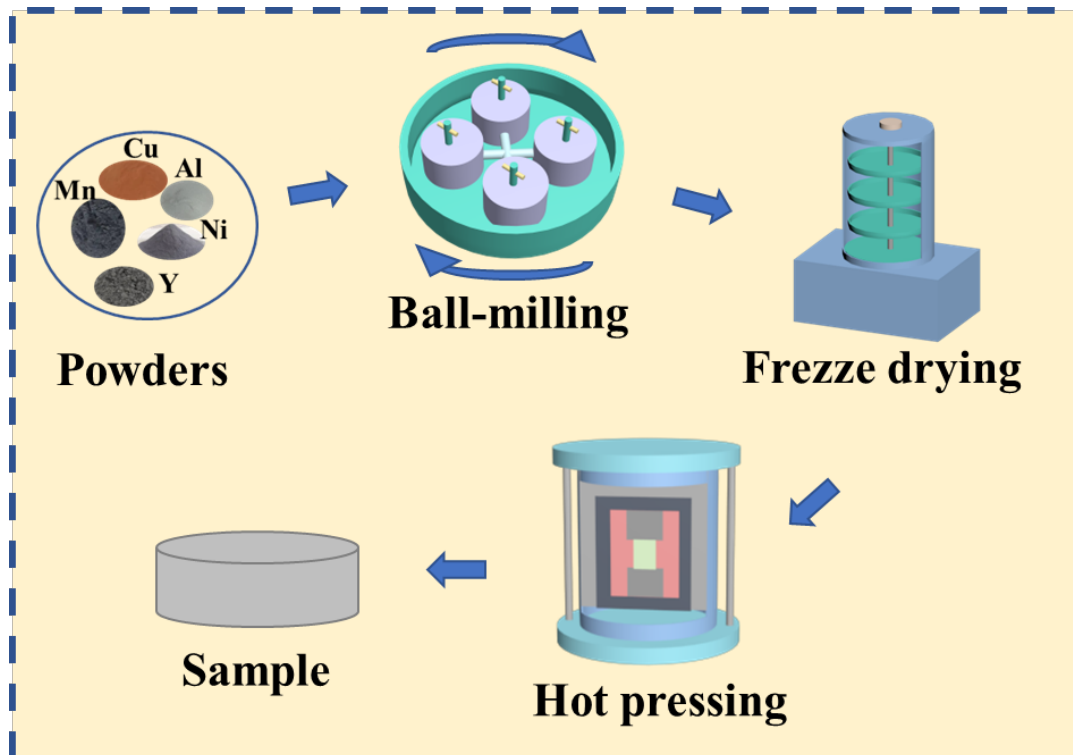


Figure 1. Preparation process of Cu-11Al-3Ni-2.5Mn-1Y alloy.

Table 1. Heat treatment temperature parameters of Cu-11Al-3Ni-2.5Mn-1Y alloy.

Number	Solution parameters	Aging parameters
#1		
#2	900 °C, 60 min	350 °C, 30 min
#3		400 °C, 30 min
#4		450 °C, 30 min
#5		500 °C, 30 min
#6		550 °C, 30 min

2.2 Phase and microstructure characterization

The phase composition and microstructure of the samples with the size of 7 mm × 7 mm × 4 mm were characterized by X-ray diffraction (XRD) and scanning electron microscopy (SEM), respectively. The phase identification was carried out by XRD (Bruker D8 Discover) in the 2θ range of 20° to 85° with Cu Kα radiation. The surface morphology was observed by SEM (JEOLJSM-7001F). The sample was polished by sandpaper and mechanical ball milling until there were no obvious scratches on the surface. In order to observe the morphology distribution more clearly, the acid solution of 3HNO₃: 1HCl: 1H₂O was used to etch the surface. To characterize the microstructure of martensite and dislocations inside the sample, the TEM samples were first cut from the RD-TD plane of the alloys with a size of 1 mm × 1 mm × 0.1 mm, and punched into a sheet with a diameter of 3 mm. Then the circle sheet was thinned by ion milling to achieve electron transparent area for transmission electron microscope (TEM) observation. The crystallographic orientation and the orientation of the crystals were determined by electron backscatter diffraction (EBSD) with a field emission scanning electron microscope (FE-SEM).

2.3 Mechanical and Damping properties characterization

The hardness was determined by microhardness tester (HXD-100TM/LCD) and kept for 10 s under 1000 g loading. The tensile strength of the samples with the size of 17 mm × 2 mm × 4 mm was measured by electronic universal testing machine (WDW-3100) at the test speed of 0.5 mm/min. The room temperature damping and high temperature damping properties were tested separately, and the sample size was

50 mm × 1.5 mm × 1.5 mm. The room temperature damping was tested in a multifunctional internal friction instrument (MFP1000) with a frequency of 1Hz and a strain amplitude of 1000×10^{-6} . The high temperature damping characteristics were characterized by Dynamic mechanical analysis instrument (TA-Q800). The range of test temperature was from 30 °C to 600 °C, frequency was 1 Hz, and the amplitude was 10 μm.

3 Experimental results and discussion

3.1 Phase identification of samples

The XRD patterns of Cu-11Al-3Ni-2.5Mn-1Y alloy after heat treatment at different temperatures are shown in Figure 2. The phase composition of the quenched specimens was 18R martensite, indicating that the ideal martensite structure is obtained after quenching. After aging at 350 °C, the peaks (111) and (019) as well as (122) and (202) corresponding to 18R martensite start to become sharp (the distance between the two peaks decreases). It indicates that the ordered reaction occurs during the process, which promotes the formation of thermoelastic martensite [30]. The 2H martensite also appears at this aging temperature. When the aging temperature increases to 400 °C, the peak strength of both 18R martensite and 2H martensite increase. Meanwhile, the peaks corresponding to (111) and (019) of 18R martensite become sharper, indicating that the aging temperature further promotes the order reaction [30]. When the aging temperature increases to 450 °C, the weak diffraction peak of γ_2 phase appears. The diffraction peak intensity of γ_2 phase increases with the elevation of temperature, indicating that the amount of γ_2 phase precipitates is increasing. The martensite phases are still the main phase, suggesting that the decomposition of the parent phase is minimal [3]. After aging at 500 °C and 550 °C, the ratio of the peak strength of 2H martensite to 18R martensite decreases, showing that there is partial conversion of 2H martensite to 18R martensite during the process. This is related to the precipitation of the γ_2 phase, which is the Al-rich phase. It leads to changes in the chemical composition with Cu-rich and Al-poor, resulting in the transformation of 2H martensite to 18R martensite [30]. Simultaneously, the shift of the peak to a higher angle indicates that part of the stress is released.

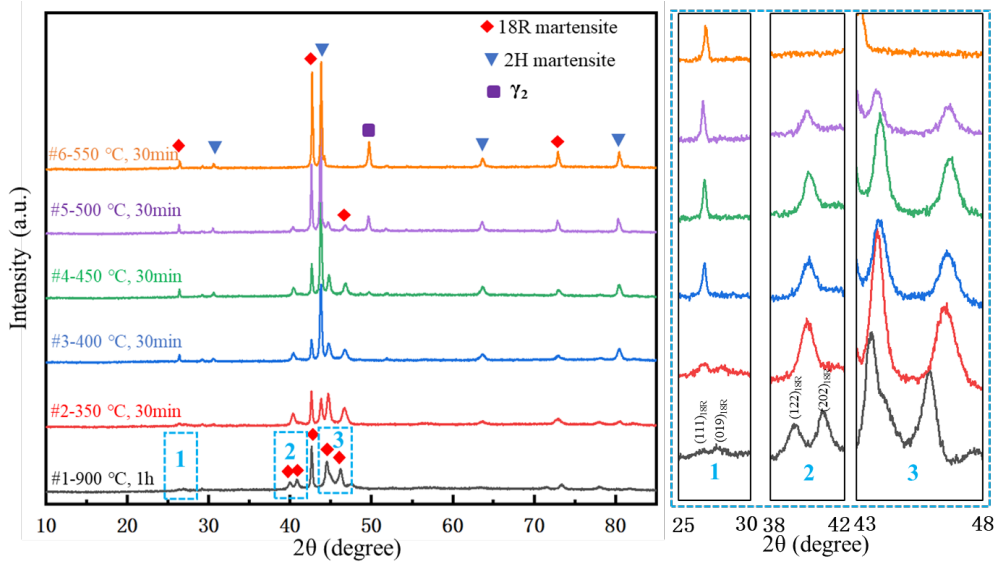


Figure 2. XRD patterns of Cu-11Al-3Ni-2.5Mn-1Y alloy with different heat treatment histories.

3.2. Microstructure analysis of samples

Figure 3 shows the scanning electron microscopy (SEM) images of Cu-11Al-3Ni-2.5Mn-1Y alloy with different heat treatment. It is obvious that martensite structures are the main phase in all samples, which is corresponding to the XRD results in Figure 2. After solution treatment at 900 °C, the martensite structure with relatively straight and clear interface was obtained. Based on the morphology and XRD results, it can be inferred that it is 18R martensite. In addition to 18R martensite, 2H martensite also appears after aging at 350 °C. The 18R martensite becomes finer and has many intersecting areas in the grains compared to the quenched state. When aging at 400 °C, the amount of 2H martensite increases without significant dimensional changes. The precipitated phase begins to appear at the grain boundary, and the two types of martensite still exist after aging at 450 °C. It means that the specimen after aging can still undergo thermoelastic martensitic phase transformation in addition to the formation of a small amount of precipitated phase. After the aging temperature was increased to 500 °C, the precipitated phase began to diffuse from the grain boundaries to the grain interior, and precipitation agglomeration appeared. According to the shape of the precipitated phase and the results of XRD, the precipitated phase is the γ_2 phase [43]. As the aging temperature increase to 550 °C, the number and size of

the precipitated phases continue to increase, and typically the excess precipitated phases will reduce the mechanical properties. Meanwhile, we can see the martensite spacing in Figure 3(e-f) is wider than Figure 3(c-d), which may be related to two factors. For one thing, the lathe/acicular type of martensite are transforming into cylindrical globules martensite can be observed. For another thing, as the aging temperature increases, the appearance and clustering of precipitated phases make the martensite alignment become dispersed, which increases the spacing between the martensite [37].

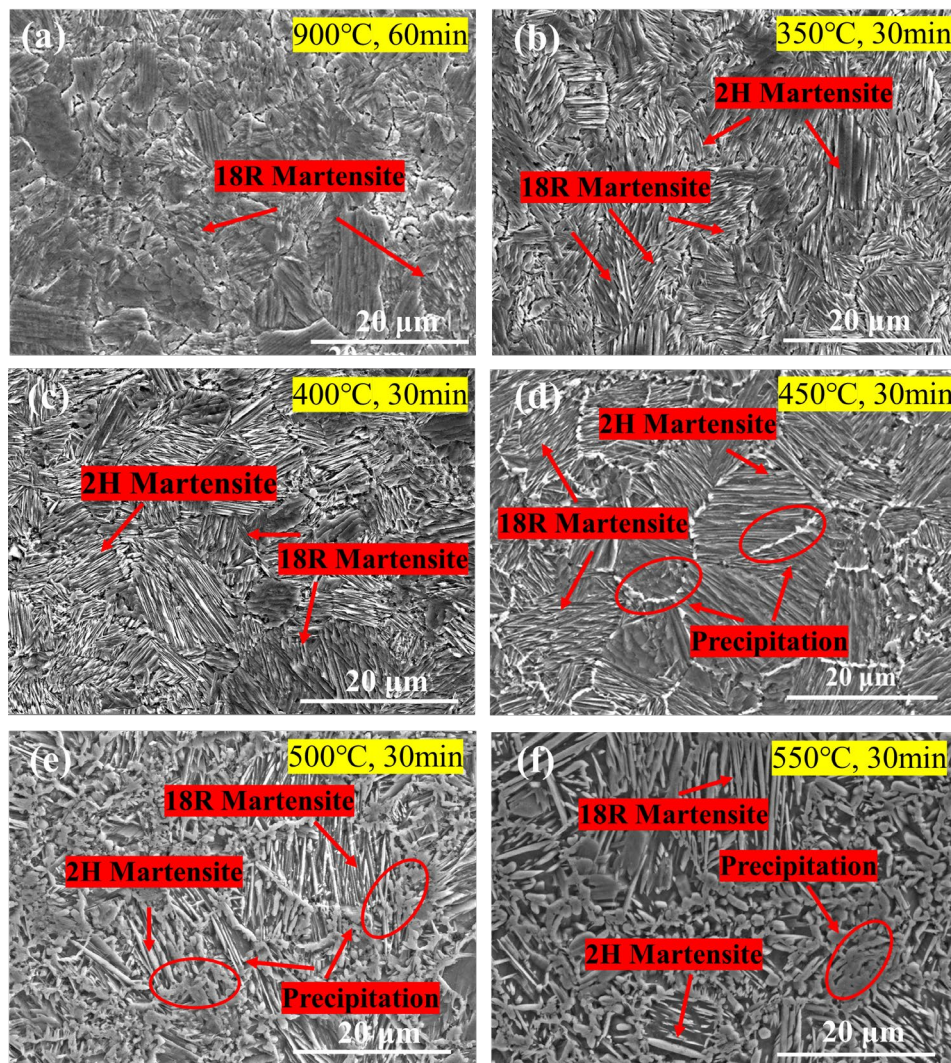


Figure 3. SEM results of Cu-11Al-3Ni-2.5Mn-1Y alloy under different heat treatment temperatures.

To further determine the grain size and grain boundary change, EBSD tests were performed on the alloy aged at 450 °C, as shown in Figure 4. The average grain size

of the sample after aging is $1.367\ \mu\text{m}$, which is significantly reduced compared with the original sample [31]. The results show that the formation of precipitation phase can effectively hinder the growth of grain. Figure 4(c) shows that the alloy is mainly composed of numerous large-angle grain boundaries and trace amounts of small-angle grain boundaries. The grain boundaries larger than 15° are called large-angle grain boundaries, and those between 2° and 15° are called small-angle grain boundaries [44]. According to the calculation results in Figure 4(d), the small-angle grain boundary accounts for only 9.2%, while the large-angle grain boundary accounts for 91.8%. The number of large-angle grain boundaries increased significantly, confirming that the grain size was remarkably refined. The large-angle grain boundaries can effectively impede the expansion of cracks and improve the toughness of the alloy.

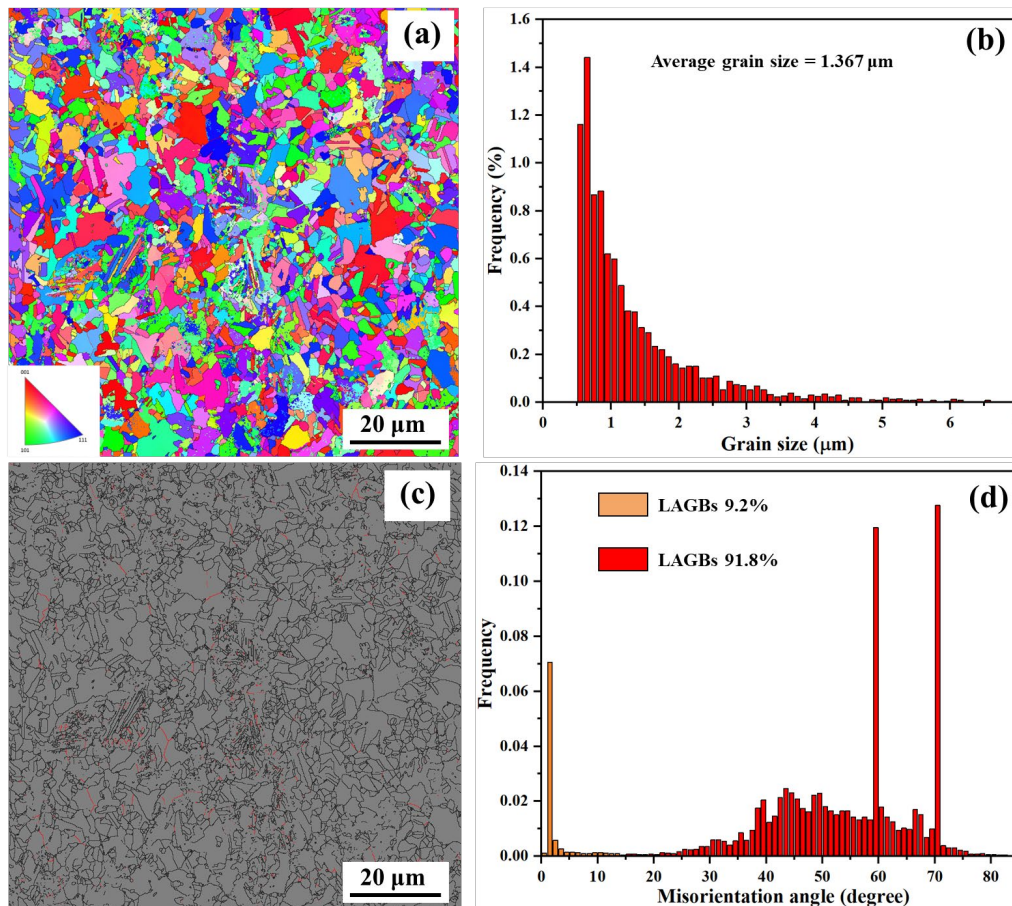


Figure 4. EBSD results of Cu-11Al-3Ni-2.5Mn-1Y alloy aged at 450 °C.

Figure 5 displays the TEM micrographs of the alloy aged at 450 °C. Figure 5(a-b) shows abundant martensite, which are 18R martensite and 2H martensite, respectively.

They inherit the ordered structure of the parent phase and are typical thermoelastic martensite. The substructures of 18R martensite and 2H martensite are stacking faults and twin structures, correspondingly. The former has a microstructure that is more adapted to movement than the latter, and is considered more thermoelastic in nature. According to the electron diffraction structures in regions A and B in Figure 5(b), the existence of both martensite is further confirmed. They provide a guarantee of good damping properties for the alloy. In addition, there are numerous aggregations of high-density dislocations, as shown in Figure 5(c-d). In general, the strong pinning effect of precipitate on dislocation is one of the main reasons for maintaining high dislocation density and leading to high strength [45, 46].

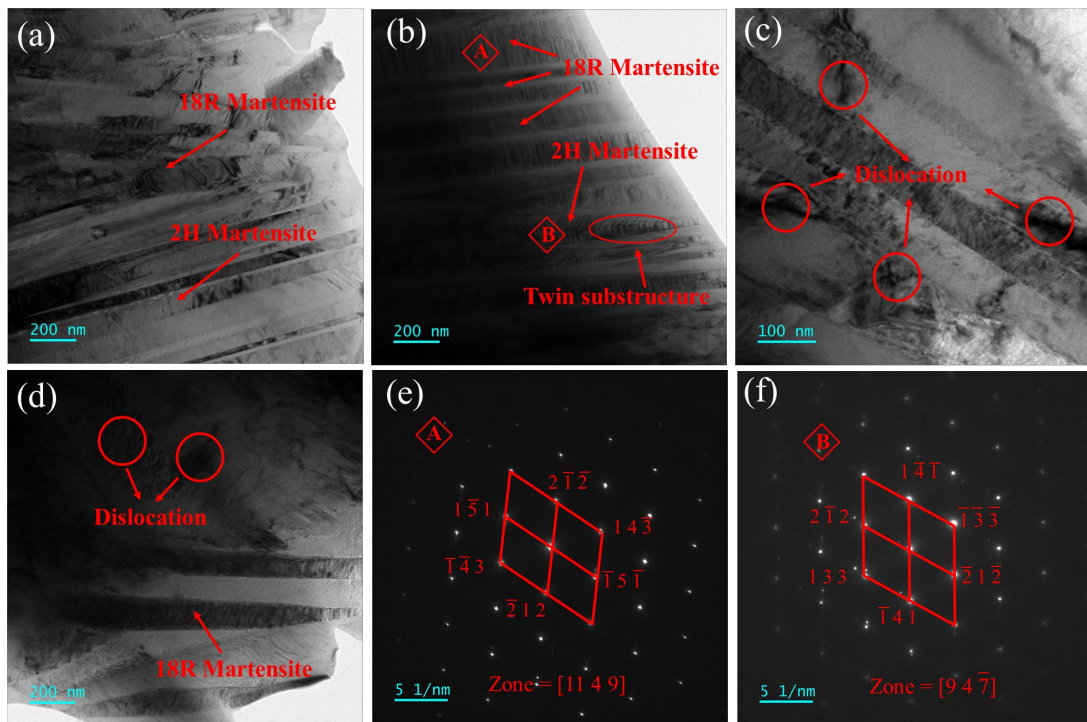


Figure 5. TEM micrographs of Cu-11Al-3Ni-2.5Mn-1Y alloy aged at 450 °C. (a-d) local bright field diagram; (e-f) corresponds to the electron diffraction results in regions A and B in Figure (b), respectively.

4 Mechanical properties and correlated mechanisms

4.1 Hardness of samples

Figure 6 shows the hardness curves of Cu-11Al-3Ni-2.5Mn-1Y alloy after solution and aging treatment at different temperatures. In previous work, the hardness of the original Cu-11Al-3Ni-2.5Mn-1Y alloy without heat treatment was 286.52 HV

[31]. There is a slight increase in the hardness after solid solution treatment at 900 °C. This is mainly due to the formation of supersaturated solid solution during the quenching process, which distorts the lattice and strengthens the alloy [45]. The hardness after aging at 350 °C is reduced compared to the solid solution treatment. This is mainly influenced by two factors. On the one hand, the increased temperature promotes the atomic motion, and the supersaturated atoms in the matrix begin to precipitate, which leads to the normal arrangement of atoms in the lattice, and finally weakens the lattice distortion and solution strengthening [47]. On the other hand, the stress formed in the quenching process will be reduced after aging, which will eventually lead to the reduction of hardness. With the increase of aging temperature, the martensite becomes finer and precipitated phase begins to form. The precipitated γ_2 phase is an electronic compound with good hardness, so the alloy has the highest hardness value after aging at 450 °C. As the aging temperature continued to increase, the phenomenon of over aging appeared. The increase in excess of γ_2 precipitated phase and agglomeration phenomenon can adversely affect the matrix organization and lead to a decrease in the hardness.

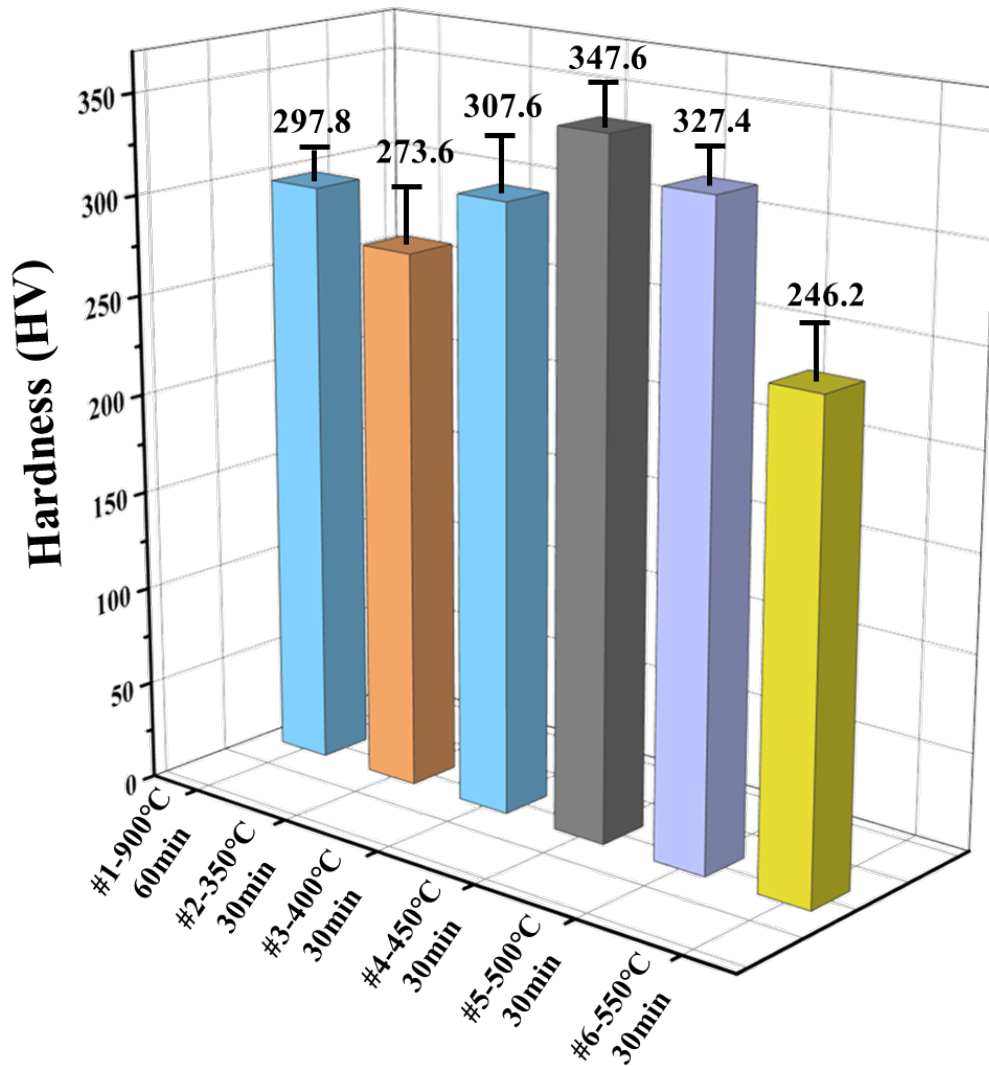


Figure 6. Hardness curves of Cu-11Al-3Ni-2.5Mn-1Y alloy after different heat treatment temperatures.

4.2 Tensile strength of samples

Figure 7 shows the tensile strength curves of Cu-11Al-3Ni-2.5Mn-1Y alloy with different temperature treatments. It is observed that the trend of strength is consistent with hardness. The curve shows that the alloy is transitioning from the elastic deformation stage to the plastic deformation stage, and fracture occurs when the external force reaches a certain value. The highest strength value of 642.6 MPa is obtained for the specimens aged at 450 °C, which is 7% higher relative to the initial sample of 601.75 MPa. The increase in strength is closely related to the precipitation of the γ_2 phase. The precipitation of γ_2 phase inhibits the grain growth and achieves fine grain strengthening, which corresponds to the EBSD results in Figure 4. At the

same time, the precipitated precipitate will inhibit the dislocation movement and realize precipitation strengthening. Combined with the inherent high strength of martensite itself, the martensite size becomes finer and therefore the strength is increased. The alloy also exhibits improved ductility, thus shows good mechanical properties. This may be due to the optimal distribution and minimum size of aging precipitates in the alloy [48]. When the aging temperature exceeds 450 °C, the excessive increase and aggregation of γ_2 phase have adverse effects on the microstructure, thus the strength begins to decrease. The strength and elongation of the alloy were significantly reduced once the aging temperature was increased to 550 °C. It shows that the over-aging phenomenon occurs and the strength of the alloy is reduced by excessive and unevenly distributed precipitated phase. As shown in Figure 3, with the increase of aging temperature, especially up to 600°C, a significant clustering of the precipitates leads to its non-uniform distribution, accompanied by an increase in the size of the precipitates. Similar phenomenon was observed in the study of Li et al. [3]. Therefore, the control of precipitated phase proportion plays an important role in alloy properties. Meanwhile, compared to the Cu-Al based alloys with strengths of 260 MPa to 440 MPa and fracture strains of 0.6% to 0.8% prepared by casting, the alloys with high strength prepared in this paper has also shown the advantage of the method [49, 50].

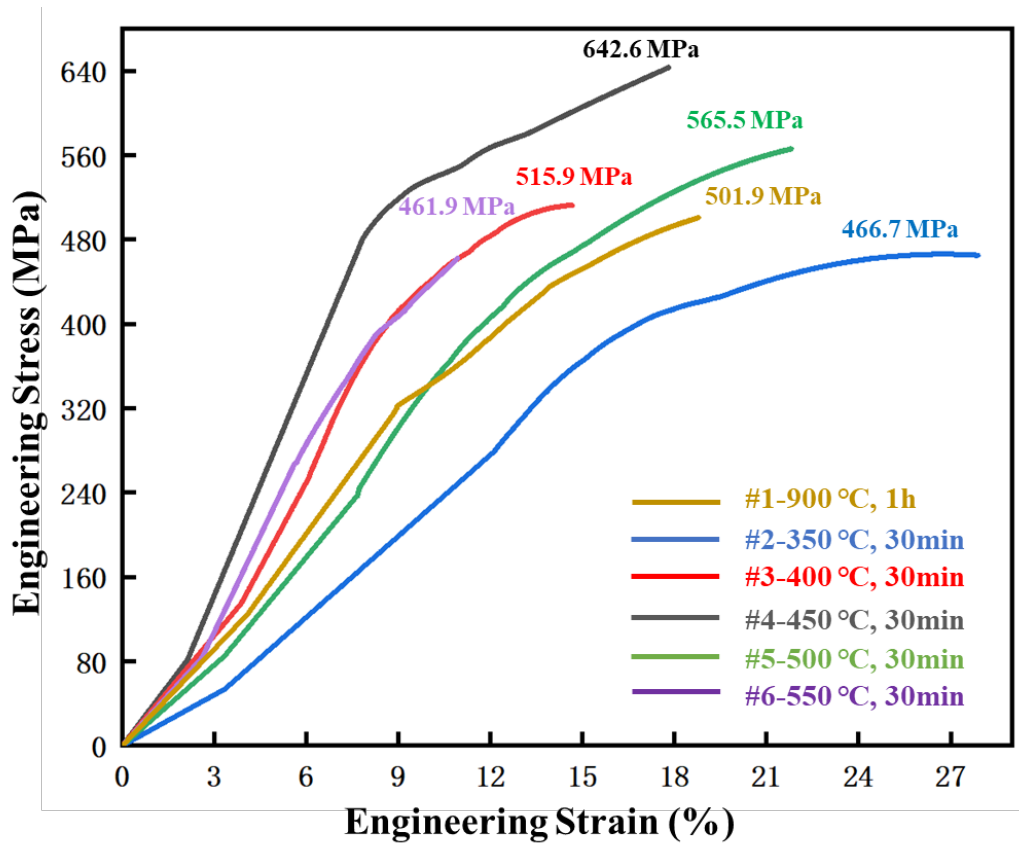


Figure 7. Engineering stress-strain curves of Cu-11Al-3Ni-2.5Mn-1Y alloy under different heat treatment temperatures.

4.3 Fracture analysis of samples

Figure 8 shows the tensile fracture morphology of Cu-11Al-3Ni-2.5Mn-1Y alloy. The fractures of all samples consist of primarily numerous dimples, showing excellent toughness. This is because under the action of tensile stress, a certain number of microscopic holes will be formed in the micro-zone range of the material. With the increase of stress and time, these microscopic holes will undergo nucleation, growing and gathering. Eventually these holes are formed and interconnected leading to fracture, which leaves dimples on the fracture surface [48, 51]. Generally, the size, number and depth of dimples affect the properties of the alloy. The larger the size and depth of the dimple will absorb more energy, thus the alloy has better plasticity [29]. After aging at 350 °C, the sample has the largest average dimple size and obvious depth, which reflects the best ductility, corresponding to the results in Figure 7. The number and size of dimples decreased obviously, indicating that the energy absorption ability of the alloy after aging at 550 °C became weaker. The gaps shown in Figure 8(f)

may act as crack sources at the beginning of fracture and develop into secondary cracks under subsequent shear stresses [51]. The appearance of a cleavage surface is also observed, indicating a decrease in the ductility, which corresponds to the result in Figure 7.

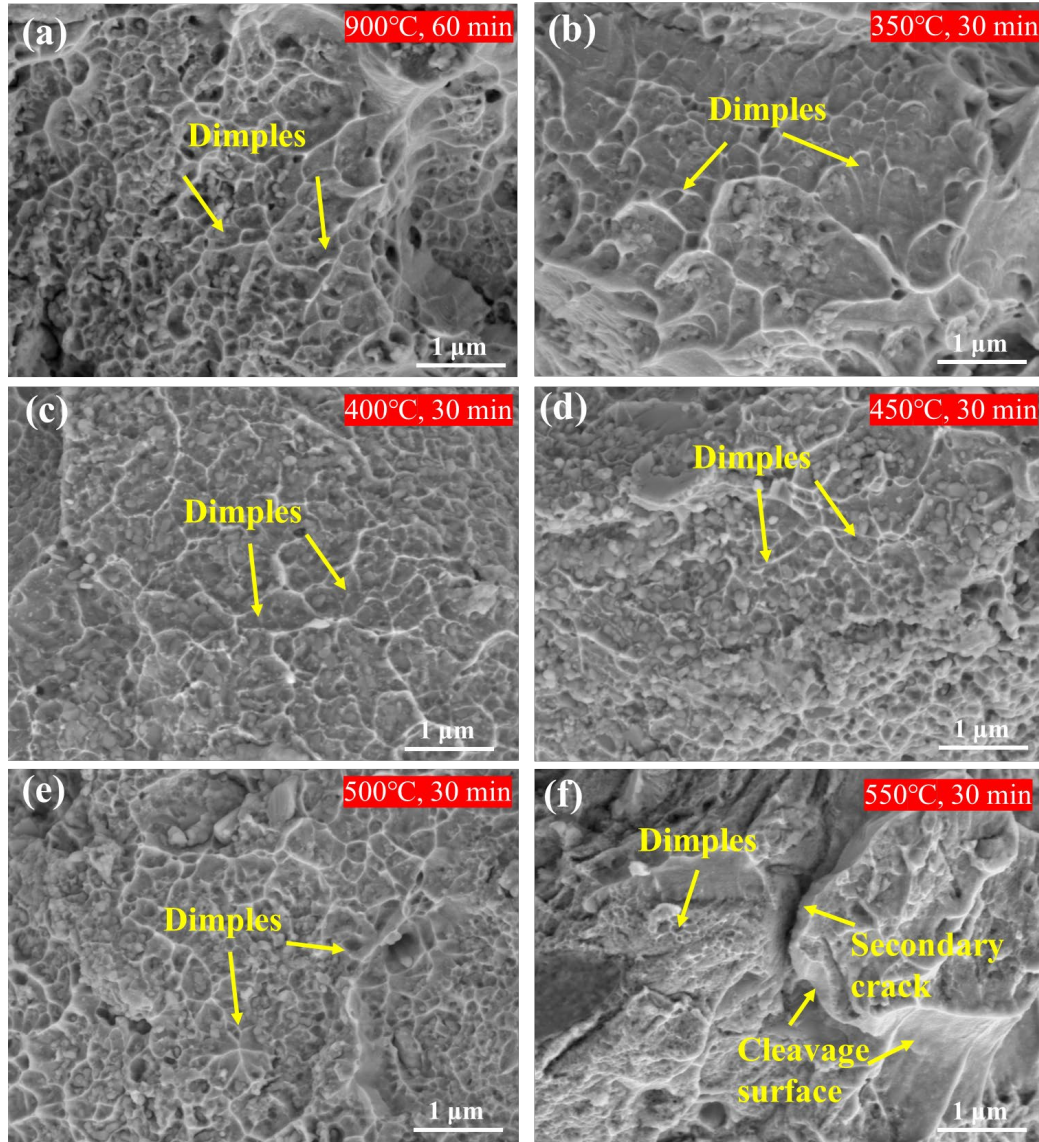


Figure 8. Tensile fracture morphology of Cu-11Al-3Ni-2.5Mn-1Y alloy treated with different temperatures.

4.4 Mechanical strengthening mechanisms

In summary, the main mechanical strengthening mechanisms involved in this paper can be described as [46, 47] :

$$\Delta\sigma = \Delta\sigma_0 + \Delta\sigma_{solution} + \Delta\sigma_{dilocation} + \Delta\sigma_{precipitation} + \Delta\sigma_{orowan} + \Delta\sigma_G$$

Where $\Delta\sigma_0$ is the inherent lattice strength of the matrix material (60 MPa for copper alloy [18]); $\Delta\sigma_{solution}$ is the solid solution strengthening effect, as shown in Figure 9(a); $\Delta\sigma_{dislocation}$ is the enhancement caused by massive dislocations; $\Delta\sigma_{precipitation}$ is the shear strengthening effect of the precipitated phase with dislocations, as shown in Figure 9(b); $\Delta\sigma_{orowan}$ is the strengthening effect caused by the precipitation phase hindering the dislocation movement, as shown in Figure 9(c); $\Delta\sigma_G$ is the grain boundary obstruction dislocation movement caused by the decrease of grain size. Meanwhile, according to the EBSD results shown in Figure 4(c-d), the alloy is mainly composed of large-angle grain boundaries, as shown in Figure 9(d). Large-angle grain boundaries can effectively prevent crack expansion and improve the toughness of the alloy [38, 44]. Toughness is a comprehensive expression of the strength and plasticity of the alloy [38], which is reflected in the improvement of the tensile strength and elongation. The massive appearance of large-angle grain boundaries also means that the grain size is significantly reduced, which is corresponding to the EBSD calculation results shown in Figure 4(b). It indicates that aging precipitation can effectively hinder the movement of grain boundaries to reduce the grain size, as shown in Figure 9(e). Therefore, combined with the above strengthening mechanisms, the optimal strength was obtained for the specimens aged at 450 °C. It demonstrates that suitable aging treatment can achieve alloys with desirable mechanical properties.

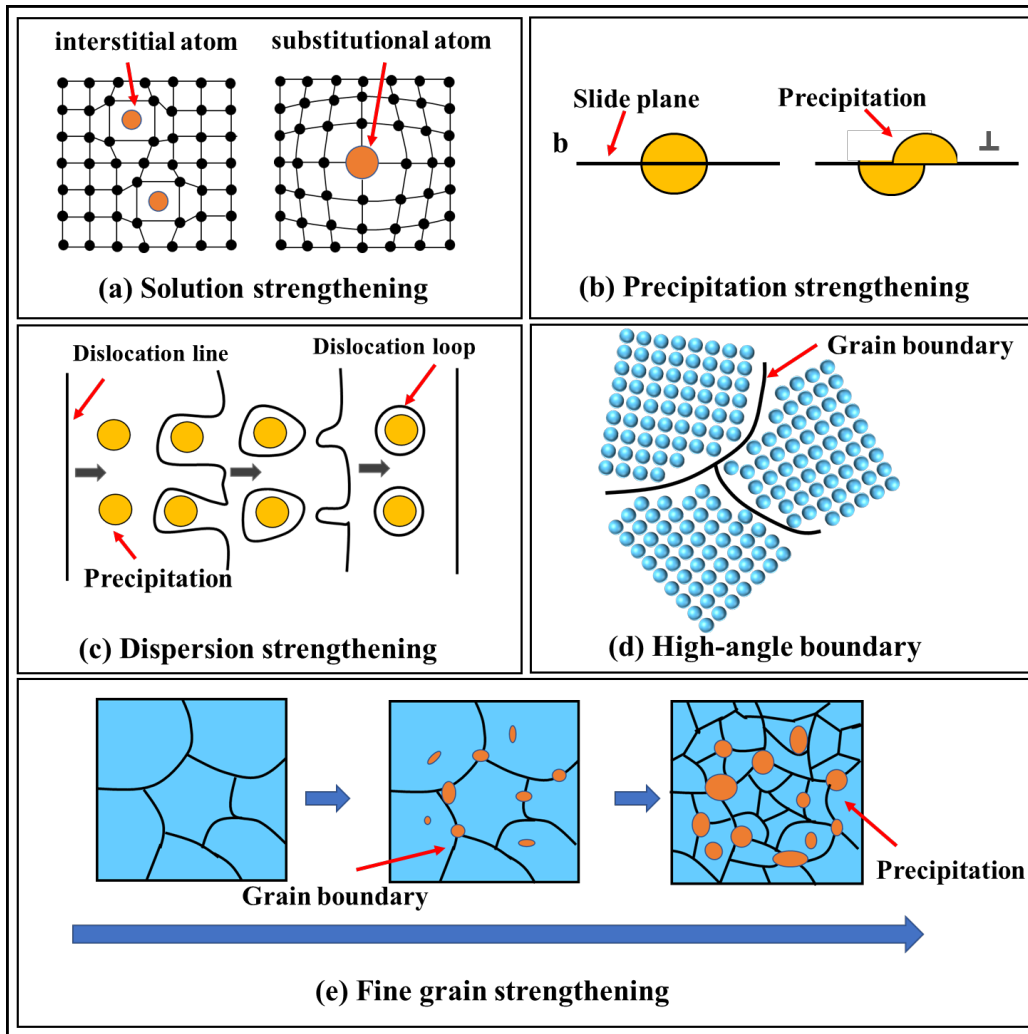


Figure 9. Main mechanical strengthening mechanisms of Cu-11Al-3Ni-2.5Mn-1Y alloy.

5 Damping behaviors and correlated mechanisms

5.1 Room temperature damping of samples

Figure 10 shows the room temperature damping curves of Cu-11Al-3Ni-2.5Mn-1Y alloy treated with different temperatures. The damping properties of all alloys increased with increasing amplitude. This is because the increase in strain amplitude facilitates the migration of various interfaces (phase interfaces, twin surfaces, and variant interfaces), thus promoting energy consumption and enhanced damping properties [52]. The damping properties of the samples treated with different temperatures are also varied. The damping value of the original samples obtained in our previous experiments is 0.038 [31]. After solution quenching at 900 °C, the presence of adverse defects (such as residual stress and vacancies) will inhibit the

motion of interface and martensite, resulting in a reduction of damping properties. When aging temperature increases from 350 °C to 450 °C, the damping property is significantly improved. This is because aging reduces the internal defects and facilitates interfacial movement to consume energy. The 18R and 2H martensite variants in the matrix are also the key sources of damping properties [53]. They are thermoelastic martensite inherited from the ordered structure of the parent phase, resulting in more twin planes and phase interfaces, which is conducive to the improvement of damping properties. The highest damping value of 0.0723 was obtained for the specimens aged at 450 °C, which was 93% higher than the original specimens and showed excellent damping properties. This is closely related to the combination of the following three factors: (1) The reduction in size of 18R martensite and 2H martensite promotes the movement of martensite interface, which facilitates energy dissipation. (2) The precipitation of γ_2 phase increases more phase interfaces for energy consumption. (3) Dislocations within the matrix contribute to part of the energy dissipation by pinning and unpinning with the precipitated phase. As the aging temperature continues to increase, the damping properties begin to decrease. This is mainly because the increase of γ_2 precipitates and agglomeration will inhibit the movement of martensite and reduce the martensite damping effect. The precipitated phase also impedes the motion of the interface and reduce the damping effect of the interface. Meanwhile, the alloy in this paper shows superior damping property, compared to other similar alloys at room temperature [3, 5, 6, 29, 54, 55], as shown in Figure 11. Therefore, the ideal damping property can be obtained by rationally setting aging parameters to control the quantity and distribution of precipitation.

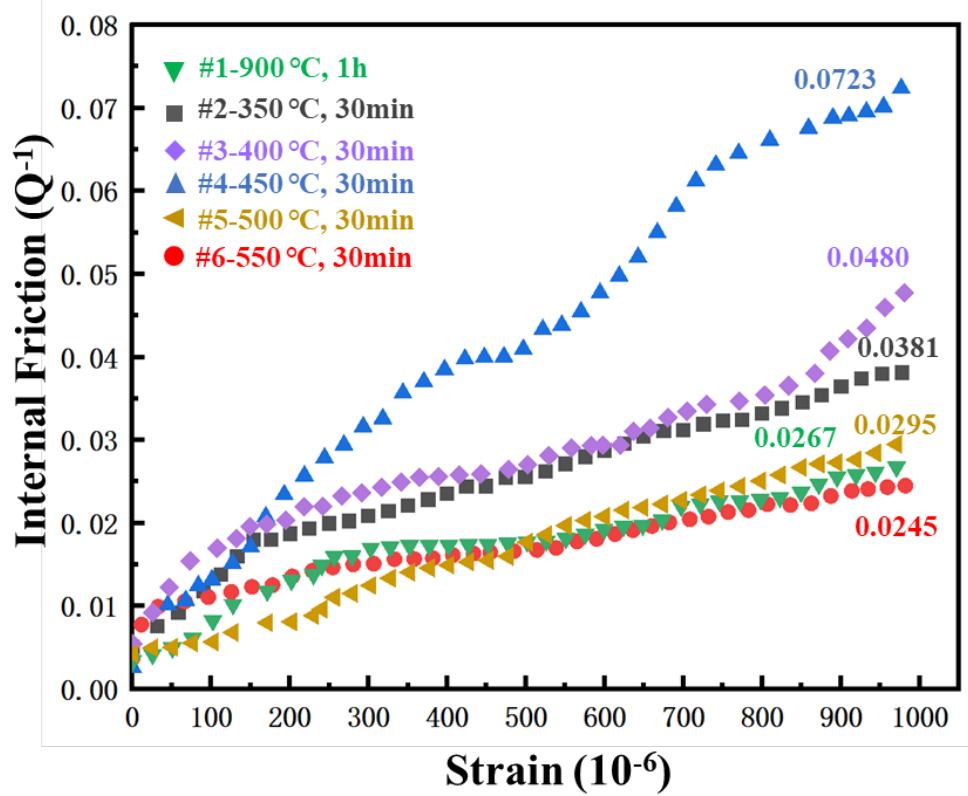


Figure 10. Room temperature damping curves of Cu-11Al-3Ni-2.5Mn-1Y alloy treated with different temperatures.

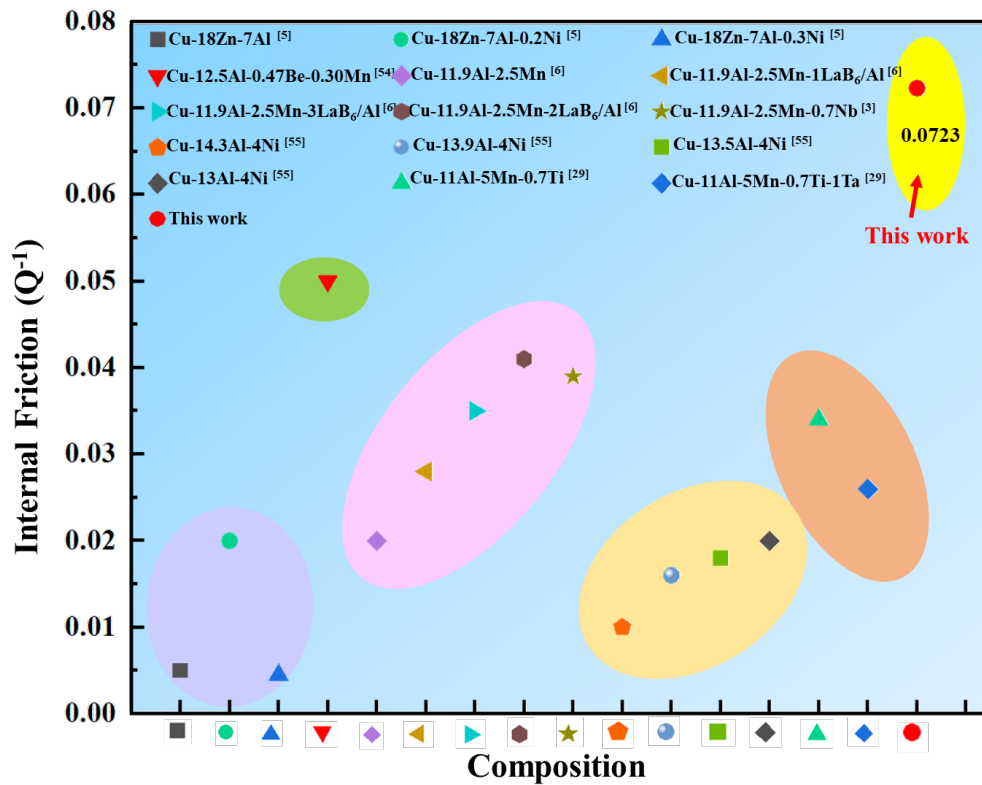


Figure 11. Comparison of damping properties at room temperature of the present Cu-11Al-3Ni-2.5Mn-1Y alloy and other similar alloys.

5.2 High temperature damping of samples

In recent years, the application of high temperature damping properties of Cu-Al-Ni based alloys has also received significant attention. The above experimental results show that the mechanical and room temperature damping properties of the alloy are remarkably improved after aging at 450 °C. The original sample and the 450 °C aged sample were characterized for high-temperature damping, as shown in Figure 12. The original sample has two damping peaks during this temperature range, which are near 150 °C and 528.6 °C. The low temperature peak is attributed to the energy dissipation of twin martensite in Cu-11Al-3Ni-2.5Mn-1Y alloy [43], while the high temperature peak originates from the reverse martensite transition. The appearance of phase transition damping peak is related to the transition from martensite to austenite. As the phase transition occurs, the increase of the phase interface and volume effects will promote energy dissipation. When the phase interface reaches the maximum value, the interface damping effect and volume effect reach the maximum value, thus the damping peak appears [56]. As the phase transition continues to increase, the number of martensite decreases and austenite increases, and damping properties begin to decrease. The damped sample aged has only one maximum value, and there is no damping peak near the low temperature. This may be related to the strong pinning effect of the γ_2 precipitation on twins. In addition, the damping values of the aged samples near 350 °C were larger than those of the original samples. This may be because the martensite becomes finer after aging, which is more conducive to interface migration. When the temperature is higher than 350 °C, the damping increase rate of aged sample is slower than that of original sample. This may be related to the pinning effect of γ_2 precipitation on the interface. In the temperature range of this test, only the maximum damping value of the aged sample appeared, and no damping peak value appeared. It can be inferred that aging at 450 °C increases the phase transition temperature of the alloy. Due to the experimental equipment, the maximum temperature can only be tested up to 600 °C, but the results are still of great reference significance.

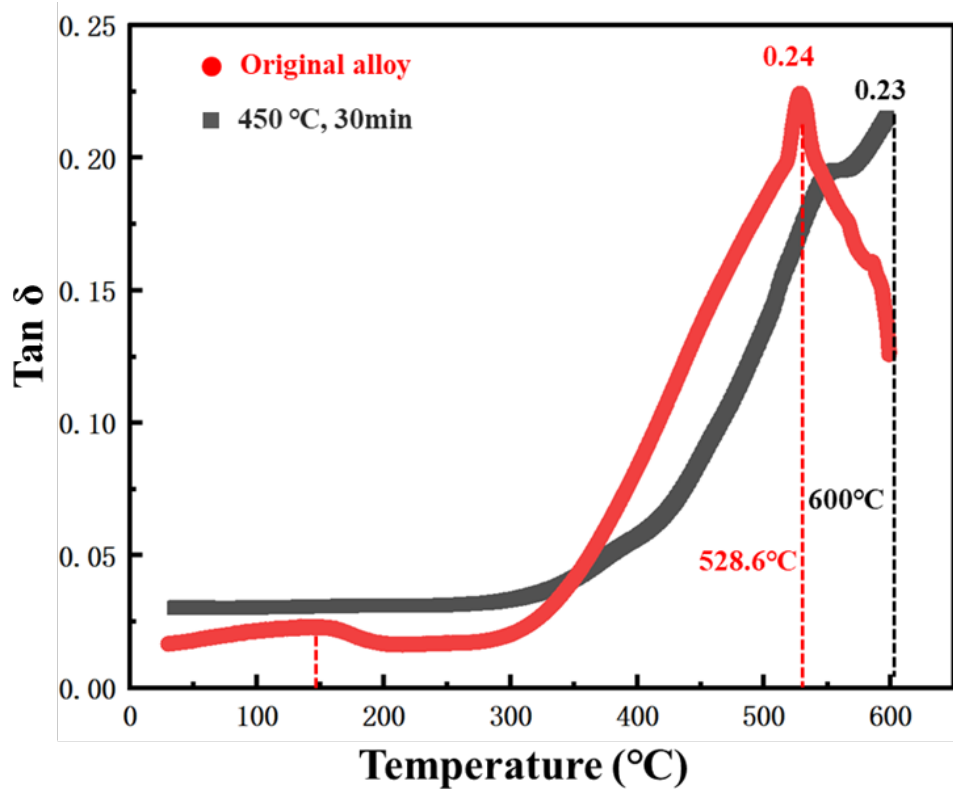


Figure 12. High temperature damping curves of Cu-11Al-3Ni-2.5Mn-1Y alloy in the original state and aged at 450 °C.

5.3 Damping strengthening mechanism

With the development of engineering applications, the damping properties of the alloy at room temperature have great research importance. The improvement of the room temperature damping properties is mainly achieved by the combined effect of the martensitic damping effect, interfacial damping effect and dislocation damping effect. Massive dislocations existed in the samples aged at 450 °C, as shown in Figure 13(a-b). Generally, the dislocation damping effect can be explained by the K-G-L model [57], as shown in Figure 13(c). When the second phase particles pin the ends of the dislocation, the dislocation damping mechanism under the action of external forces can be divided into two types. They are amplitude-independent vibration damping as shown in equation (1-1) and amplitude-dependent static hysteresis damping as shown in equations (1-2)-(1-4) [57].

$$\tan\Phi = \frac{\Delta BL^4\omega}{36Gb^2} \quad (1-1)$$

Where Λ is dislocation density; B is a constant; L is the length of the pinned dislocation; ω is the angular frequency; G is the shear modulus of the alloy; B is the Burgundy vector of the alloy.

$$Q^{-1} = \frac{c_1}{\varepsilon_0} \exp\left(-\frac{c_2}{\varepsilon_0}\right) \quad (1-2)$$

$$c_1 = \frac{\Omega \Delta_0 \Lambda L_n^3}{\pi^2 L_c} \quad (1-3)$$

$$c_2 = \frac{ka\delta}{L_c} \quad (1-4)$$

Where ε_0 is the strain amplitude of the alloy, Ω is the orientation parameter of the dislocation in the slip system, $\Delta_0 = \frac{4(1-\nu)}{\pi^2}$ is Poisson's ratio, Λ is the dislocation density, L_n is the maximum length of the dislocation pinned, L_c is the minimum average length of the dislocation pinned, k is a constant, a is the lattice constant, δ is the ratio of the size of the pinned solute atom to the solvent atom, c_1 is proportional to the dislocation density.

The precipitated phase formed in the age-treated Cu-11Al-3Ni-2.5Mn-1Y alloy prevents the movement of dislocations, as shown in Figure 13(c). Under the action of sufficiently large external force, the dislocation line pinned by the precipitate phase will bend to a certain extent. The movement of the dislocation can consume energy to contribute partial damping properties. Under the combined action of applied and residual thermal stress, it exhibits damping properties related to strain amplitude [1]. In this case, various defects in the alloy will become the pinning points of dislocations, which can be divided into immobile strong pinning points (such as precipitated phase and grain boundary) and mobile weak pinning points (such as impurity atoms and vacancies) [58]. Under the maximum stress, the dislocation in Cu-11Al-3Ni-2.5Mn-1Y alloy will break away from the weak pinning points (such as vacancies) and be inhibited by the strong pinning points (such as precipitate phase and grain boundary) to form dislocation rings. During this process dislocations consume energy through pinning and unpinning, significantly improving the damping properties of the alloy. Therefore, the Cu-11Al-3Ni-2.5Mn-1Y alloy exhibits good room temperature damping properties under the combined effect of the above microstructure.

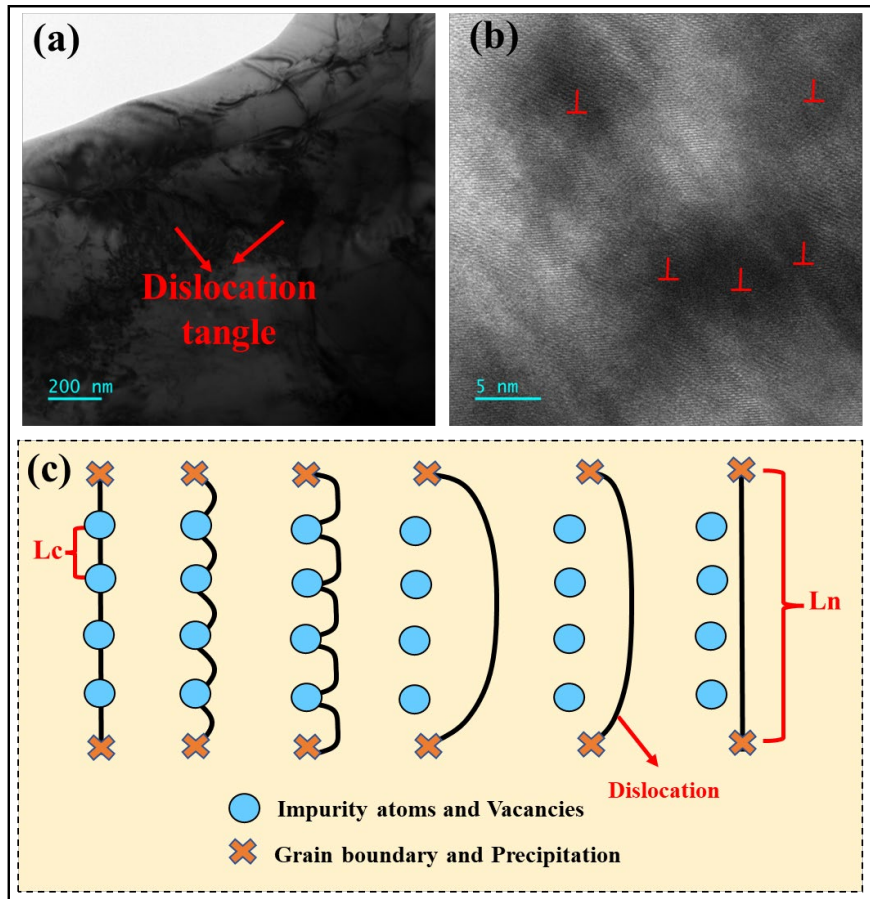


Figure 13. (a-b) TEM image of the sample aged at 450 °C; (c) Dislocation damping effect.

6 Conclusion

In this paper, the Cu-11Al-3Ni-2.5Mn-1Y alloy prepared by hot-press sintering was subjected to aging treatment at different temperatures. The effects of different aging temperatures on the microstructure, mechanical and damping properties of Cu-11Al-3Ni-2.5Mn-1Y alloy were studied. The conclusions are as follows:

(1) The alloy after aging treatment is mainly composed of 18R martensite and 2H martensite. The γ_2 phase is formed in the specimens aged at 450 °C, and the amount of γ_2 phase increases with the increase of temperature.

(2) After aging at 450 °C, the strength of the alloy increases to 642.6 MPa. This is mainly due to the lattice distortion and dislocation increment effect caused by solution strengthening, the shear and obstruction effect of precipitated phase and dislocation, the fine grain strengthening effect caused by grain size reduction, and the increase of large-angle grain boundaries.

(3) After aging at 450 °C, the damping peak reaches 0.0723, which is 93% higher than that of the original sample. This is mainly caused by the change in the number and size of martensite, the interfacial damping effect caused by the precipitated phase, and the pinning and unpinning reactions between dislocations and the precipitated phase.

(4) In this experiment, the mechanical and damping properties of the alloy aged at 450 °C were significantly improved. The results show that appropriate aging treatment can improve the mechanical and damping properties simultaneously, which is expected to promote the application and development of Cu-Al based alloys in more fields.

Conflict of interest

The authors declare that they have no conflict of interest.

Acknowledgments

This work was supported by Key Laboratory of Infrared Imaging Materials and Detectors, Shanghai Institute of Technical Physics, Chinese Academy of Sciences (No.IIMDKFJJ-21-10), China Postdoctoral Science Foundation (No. 2018T110993).

Data Availability statement

The data used to support the findings of this study are available from the corresponding author upon request.

Reference

- [1] Jiang Z, Wang F, Yin J, Gong S, Dai Z, Pang Y, Xiong Y, Zhu Z, Li Z, Vibration damping mechanism of CuAlMn/polymer/carbon nanomaterials multi-scale composites, *Composites Part B: Engineering*. 199 (2020) 108266. <https://doi.org/10.1016/j.compositesb.2020.108266>.
- [2] Wang Q, Han F, Cui C, Effect of heat treatment on the two internal friction peaks in a Cu–Al–Mn shape memory alloy, *Journal of Alloys and Compounds*. 492 (1-2) (2010) 286-290. <https://doi.org/10.1016/j.jallcom.2009.11.072>.
- [3] Li H, Wang Q, Yin F, Cui C, Hao G, Jiao Z, Zheng N, Effects of Parent Phase Aging and Nb Element on the Microstructure, Martensitic Transformation, and Damping Behaviors of a Cu–Al–Mn Shape Memory Alloy, *physica status solidi (a)*. 217 (6) (2020) 1900923. <https://doi.org/10.1002/pssa.201900923>.
- [4] Sutou Y, Omori T, Wang JJ, Kainuma R, Ishida K, Characteristics of Cu–Al–Mn-based shape memory alloys and their applications, *Materials Science and Engineering: A*. 378 (1-2) (2004) 278-282. <https://doi.org/10.1016/j.msea.2003.12.048>.
- [5] Alaneme KK, Umar S, Mechanical behaviour and damping properties of Ni modified Cu–Zn–Al shape memory alloys, *Journal of Science: Advanced Materials and Devices*. 3 (3) (2018) 371-379. <https://doi.org/10.1016/j.jsamd.2018.05.002>.
- [6] liu X, Wang Q, Kondrat'ev SY, Ji P, Yin F, Cui C, Hao G, Microstructural, Mechanical, and Damping Properties of a Cu-Based Shape Memory Alloy Refined by an In Situ LaB₆/Al Inoculant, *Metallurgical and Materials Transactions A*. 50 (5) (2019) 2310-2321. <https://doi.org/10.1007/s11661-019-05153-9>.
- [7] Santosh S, Kevin T, Rajkumar K, Sabareesh A, Effect of Ni and Mn additions on the damping characteristics of Cu-Al-Fe based high temperature shape memory alloys, *Journal of Alloys and Compounds*. 924 (2022) 166258. <https://doi.org/10.1016/j.jallcom.2022.166258>.
- [8] Meng X, Zhang D, Zhang W, Qiu C, Chen D, Achieving high damping capacity and strength simultaneously in a high-zinc aluminum alloy via melt spinning and hot extrusion, *Materials Science and Engineering: A*. 833 (2022) 142376. <https://doi.org/10.1016/j.msea.2021.142376>.
- [9] Jiao Z, Wang Q, Yin F, Zhang J, Liu L, Ji P, Chu H, Yu J, Novel laminated multi-layer graphene/Cu–Al–Mn composites with ultrahigh damping capacity and superior tensile mechanical properties, *Carbon*. 188 (2022) 45-58. <https://doi.org/10.1016/j.carbon.2021.11.055>.
- [10] Zhao Y, Ning R, Sun S, Wang H, Gao Y, Gao Z, Cai W, Achieved improvement of damping capacity in Ti Ni shape memory alloy through He-ion irradiation, *Materials Characterization*. 180 (2021). <https://doi.org/10.1016/j.matchar.2021.111417>.
- [11] Yoshida I, Monma D, Iino K, Ono T, Otsuka K, Asai M, Internal friction of Ti–Ni–Cu ternary shape memory alloys, *Materials Science and Engineering: A*. 370(1-2) (2004) 444-448. <https://doi.org/10.1016/j.msea.2003.05.003>.
- [12] Zhao C, Yang J, Li G, Wang Z, Laser powder bed fusion of the Mn-Cu alloys: Printability, microstructure, and mechanical properties, *Journal of Alloys and Compounds*. 899 (2022) 163385. <https://doi.org/10.1016/j.jallcom.2021.163385>.

- [13] Fukuhara M, Yin F, Ohsawa Y, Takamori S, High-damping properties of Mn–Cu sintered alloys, *Materials Science and Engineering: A*. 442 (1-2) (2006) 439-443. <https://doi.org/10.1016/j.msea.2006.05.163>.
- [14] Zhang L, Jiang X, Sun H, Zhang Y, Fang Y, Shu R, Microstructure, mechanical properties and damping capacity of Fe-Mn-Co Alloys reinforced with graphene, *Journal of Alloys and Compounds*. 931 (2023) 167547. <https://doi.org/10.1016/j.jallcom.2022.167547>.
- [15] Wang H, Wang H, Zhang R, Liu R, Xu Y, Tang R, Effect of high strain amplitude and pre-deformation on damping property of Fe-Mn alloy, *Journal of Alloys and Compounds*. 770 (2019) 252-256. <https://doi.org/10.1016/j.jallcom.2018.08.099>.
- [16] Xu X-Q, Xu Y-Q, Higher damping capacity induced by negative magnetostriction of Fe-16Cr-2.5Mo-0~0.2V alloys, *Journal of Alloys and Compounds*. 852 (2021) 156673. <https://doi.org/10.1016/j.jallcom.2020.156673>.
- [17] Mohamed AK, Zadorozhnyy MY, Mansouri Y, Golovin IS, Magnetostriction and damping of forced vibrations in Fe-Cr-Mo-Al alloy, *Materials Letters*. 314 (2022) 131863. <https://doi.org/10.1016/j.matlet.2022.131863>.
- [18] Wang M, Zhang R, Xiao Z, Gong S, Jiang Y, Li Z, Microstructure and properties of Cu-10 wt%Fe alloy produced by double melt mixed casting and multi-stage thermomechanical treatment, *Journal of Alloys and Compounds*. 820 (2020) 153323. <https://doi.org/10.1016/j.jallcom.2019.153323>.
- [19] Araki Y, Endo T, Omori T, Sutou Y, Koetaka Y, Kainuma R, Ishida K, Potential of superelastic Cu-Al-Mn alloy bars for seismic applications, *Earthquake Engineering & Structural Dynamics*. 40(1) (2011) 107-115. <https://doi.org/10.1002/eqe.1029>.
- [20] Agrawal A, Dube RK, Methods of fabricating Cu-Al-Ni shape memory alloys, *Journal of Alloys and Compounds*. 750 (2018) 235-247. <https://doi.org/10.1016/j.jallcom.2018.03.390>.
- [21] Saud SN, Hamzah E, Abubakar T, Bakhsheshi-Rad HR, Farahany S, Abdolahi A, Taheri MM, Influence of Silver nanoparticles addition on the phase transformation, mechanical properties and corrosion behaviour of Cu–Al–Ni shape memory alloys, *Journal of Alloys and Compounds*. 612 (2014) 471-478. <https://doi.org/10.1016/j.jallcom.2014.05.173>.
- [22] Karagoz Z, Canbay CA, Relationship between transformation temperatures and alloying elements in Cu–Al–Ni shape memory alloys, *Journal of Thermal Analysis and Calorimetry*. 114 (3) (2013) 1069-1074. <https://doi.org/10.1007/s10973-013-3145-9>.
- [23] Shafeeq M, Gupta GK, Hirshikesh, Malik MM, Modi OP, Effect of milling parameters on processing, microstructure and properties of Cu–Al–Ni–Ti shape memory alloys, *Powder Metallurgy*. 58 (4) (2015) 265-272. <https://doi.org/10.1179/1743290115y.0000000002>.
- [24] Adorno AT, Silva RAG, Ageing behavior in the Cu–10wt.%Al and Cu–10wt.%Al–4wt.%Ag alloys, *Journal of Alloys and Compounds*. 473 (1-2) (2009) 139-144. <https://doi.org/10.1016/j.jallcom.2008.05.072>.
- [25] Vajpai SK, Dube RK, Sangal S, Microstructure and properties of Cu–Al–Ni shape memory alloy strips prepared via hot densification rolling of argon atomized

- powder preforms, *Materials Science and Engineering: A*. 529 (2011) 378-387. <https://doi.org/10.1016/j.msea.2011.09.046>.
- [26] Fu H, Xu S, Zhao H, Dong H, Xie J, Cyclic stress-strain response of directionally solidified polycrystalline Cu-Al-Ni shape memory alloys, *Journal of Alloys and Compounds*. 714 (2017) 154-159. <https://doi.org/10.1016/j.jallcom.2017.04.234>.
- [27] Sampath V, Studies on the effect of grain refinement and thermal processing on shape memory characteristics of Cu–Al–Ni alloys, *Smart Materials and Structures*. 14 (5) (2005) S253-S260. <https://doi.org/10.1088/0964-1726/14/5/013>.
- [28] Zhang Q, Cui B, Sun B, Zhang X, Dong Z, Liu Q, Cui T, Effect of Sm Doping on the Microstructure, Mechanical Properties and Shape Memory Effect of Cu-13.0Al-4.0Ni Alloy, *Materials (Basel)*. 14 (14) (2021) 144007. <https://doi.org/10.3390/ma14144007>.
- [29] Yang L, Jiang X, Sun H, Shao Z, Fang Y, Shu R, Effect of Ta addition on microstructures, mechanical and damping properties of Cu–Al–Mn–Ti alloy, *Journal of Materials Research and Technology*. 15 (2021) 3825-3835. <https://doi.org/10.1016/j.jmrt.2021.10.031>.
- [30] Yang L, Jiang X, Sun H, Shao Z, Fang Y, Shu R, Effects of alloying, heat treatment and nanoreinforcement on mechanical properties and damping performances of Cu–Al-based alloys: A review, *Nanotechnology Reviews*. 10 (1) (2021) 1560-1591. <https://doi.org/10.1515/ntrev-2021-0101>.
- [31] Yang L, Jiang X, Sun H, Shao Z, Fang Y, Shu R, Effect of Y on microstructure, damping properties and mechanical properties of Cu-Al-Ni-Mn alloy, *Materials Letters*. 308 (2022) 131170. <https://doi.org/10.1016/j.matlet.2021.131170>.
- [32] Wang QZ, Lu DM, Cui CX, Liu WJ, Xu M, Yang J, Effects of aging on the structure and damping behaviors of a novel porous CuAlMn shape memory alloy fabricated by sintering–dissolution method, *Materials Science and Engineering: A*. 615 (2014) 278-282. <https://doi.org/10.1016/j.msea.2014.07.080>.
- [33] Dalvand P, Raygan S, López GA, Meléndez MB, Chernenko VA, Effect of Aging on the Structure and Transformation Behavior of Cu–12Al–3.5Ni–0.7Ti–0.05RE High Temperature Shape Memory Alloy, *Metals and Materials International*. 26 (9) (2019) 1354-1365. <https://doi.org/10.1007/s12540-019-00376-2>.
- [34] Saud SN, Hamzah E, Abubakar T, Bakhsheshi-Rad HR, Hosseinian R, X-phase precipitation in aging of Cu–Al–Ni–xTi shape memory alloys and its influence on phase transition behavior, *Journal of Thermal Analysis and Calorimetry*. 123 (1) (2015) 377-389. <https://doi.org/10.1007/s10973-015-4894-4>.
- [35] Yang Q, Wang SL, Chen J, Zhou TN, Peng HB, Wen YH, Strong heating rate-dependent deterioration of shape memory effect in up/step quenched Cu-based alloys: A ductile Cu Al Mn alloy as an example, *Acta Materialia*. 111 (2016) 348-356. <https://doi.org/10.1016/j.actamat.2016.04.004>.
- [36] Mallik US, Sampath V, Effect of composition and ageing on damping characteristics of Cu–Al–Mn shape memory alloys, *Materials Science and Engineering: A*. 478 (1-2) (2008) 48-55. <https://doi.org/10.1016/j.msea.2007.05.073>.

- [37] Milhorato FR, Mazzer EM, Effects of aging on a spray-formed Cu-Al-Ni-Mn-Nb high temperature shape memory alloy, *Materials Science and Engineering: A*. 753 (2019) 232-237. <https://doi.org/10.1016/j.msea.2019.03.024>.
- [38] Yang S, Chi M, Zhang J, Lu Y, Huang Y, Wang C, Liu X, Abnormal grain growth in annealing cast Cu–Al–Mn–V alloys and their superelasticity, *Smart Materials and Structures*. 28 (5) (2019) 055015. <https://doi.org/10.1088/1361-665X/ab0b73>.
- [39] Chentouf SM, Bouabdallah M, Cheniti H, Eberhardt A, Patoor E, Sari A, Ageing study of Cu–Al–Be hypoeutectoid shape memory alloy, *Materials Characterization*. 61 (11) (2010) 1187-1193. <https://doi.org/10.1016/j.matchar.2010.07.009>.
- [40] Kumar N, Bharti A, Saxena KK, A re-investigation: Effect of powder metallurgy parameters on the physical and mechanical properties of aluminium matrix composites, *Materials Today: Proceedings*. 44 (2021) 2188-2193. <https://doi.org/10.1016/j.matpr.2020.12.351>.
- [41] Qu Z, Zhang P, Liang S, Lai Y, Luo C, Deformation Behavior of Superalloy Powder Compact under Hot Isostatic Pressing, *Advanced Engineering Materials*. 22 (11) (2020) 2000534. <https://doi.org/10.1002/adem.202000534>.
- [42] Wu Z, Jiang X, Li Y, Christian P, Sun H, Zhang Y, Fang Y, Shu R, Microstructures and properties of graphene nanoplatelets reinforced Cu/Ti₃SiC₂/C nanocomposites with efficient dispersion and strengthening achieved by high-pressure torsion, *Materials Characterization*. 193 (2022) 112308. <https://doi.org/10.1016/j.matchar.2022.112308>.
- [43] Jiao Z, Wang Q, Yin F, Cui C, Effect of precipitation during parent phase aging on the microstructure and properties of a refined CuAlMn shape memory alloy, *Materials Science and Engineering: A*. 737 (2018) 124-131. <https://doi.org/10.1016/j.msea.2018.09.037>.
- [44] Liu J-l, Chen ZH, Huang H-y, Xie J-x, Microstructure and superelasticity control by rolling and heat treatment in columnar-grained Cu-Al-Mn shape memory alloy, *Materials Science and Engineering: A*. 696 (2017) 315-322. <https://doi.org/10.1016/j.msea.2017.04.085>.
- [45] Dai J, Ma M, Xiao Z, Meng X, Sun G, Zhang T, Zhou T, Li L, Zhu Y, Effect of trace silicon addition on microstructure and properties of a Cu–0.26Cr–0.14Mg alloy, *Materials Science and Engineering: A*. 833 (2022) 142511. <https://doi.org/10.1016/j.msea.2021.142511>.
- [46] Dudova N, Plotnikova A, Molodov D, Belyakov A, Kaibyshev R, Structural changes of tempered martensitic 9%Cr–2%W–3%Co steel during creep at 650°C, *Materials Science and Engineering: A*. 534 (2012) 632-639. <https://doi.org/10.1016/j.msea.2011.12.020>.
- [47] Wang X, Xiao Z, Qiu W-t, Li Z, Liu F, The evolution of microstructure and properties of a Cu–Ti–Cr–Mg–Si alloy with high strength during the multi-stage thermomechanical treatment, *Materials Science and Engineering: A*. 803 (2021) 140510. <https://doi.org/10.1016/j.msea.2020.140510>.
- [48] Zhang Z, Ma X, Zhang C, Chu G, Meng Z, Zhao G, Chen L, Effect of stress-aging treatment on the mechanical and corrosion properties of Al–Zn–Mg–Cu alloy,

- Materials Science and Engineering: A. 838 (2022) 142791. <https://doi.org/10.1016/j.msea.2022.142791>.
- [49] Leu S.S, Chen Y.C, Jean R.D, Effect of rapid solidification on mechanical properties of Cu-Al-Ni shape memory alloys, *Journal Materials Science*. 27 (1992) 2792–2798. <https://doi.org/10.1007/BF00540706>.
- [50] Duerig T.W, Albrecht J, Gessinger G.H, A Shape-Memory Alloy for High-Temperature Applications, *Journal Of Metals*. 34 (1982) 14–20. <https://doi.org/10.1007/BF03338156>.
- [51] Zhang Q, Zhang C, Lin J, Zhao G, Chen L, Zhang H, Microstructure analysis and low-cycle fatigue behavior of spray-formed Al–Li alloy 2195 extruded plate, *Materials Science and Engineering: A*. 742 (2019) 773-787. <https://doi.org/10.1016/j.msea.2018.11.053>.
- [52] Liu Y, Yin F, Yu H, Feng J, Ji P, Zhang J, Jiao Z, Liu L, Wang Q, Microstructural evolution, damping and tensile mechanical properties of multilayer Zn–22Al alloy fabricated by accumulative roll bonding (ARB), *Materials Science and Engineering: A*. 840 (2022) 142911. <https://doi.org/10.1016/j.msea.2022.142911>.
- [53] Ueland SM, Schuh CA, Transition from many domain to single domain martensite morphology in small-scale shape memory alloys, *Acta Materialia*. 61 (15) (2013) 5618-5625. <https://doi.org/10.1016/j.actamat.2013.06.003>.
- [54] Shivasiddaramaiah AG, Mallik US, Shivaramu L, Prashantha S, Evaluation of shape memory effect and damping characteristics of Cu–Al–Be–Mn shape memory alloys, *Perspectives in Science*. 8 (2016) 244-246. <https://doi.org/10.1016/j.pisc.2016.04.041>.
- [55] Chang SH, Influence of chemical composition on the damping characteristics of Cu–Al–Ni shape memory alloys, *Materials Chemistry and Physics*. 125 (3) (2011) 358-363. <https://doi.org/10.1016/j.matchemphys.2010.09.077>.
- [56] Wang J, Jin Y, Wu R, Wang D, Qian B, Zhang J, Hou L, Simultaneous improvement of strength and damping capacities of Mg-8Li-6Y–2Zn alloy by heat treatment and hot rolling, *Journal of Alloys and Compounds*. 927 (2022) 167027. <https://doi.org/10.1016/j.jallcom.2022.167027>.
- [57] Zhou Z, Li H, Liu Y, Chen S, Niu T, Li H, Effect of Ti addition on the damping and mechanical properties of solid-solution FeCrCoNi alloys, *Journal of Alloys and Compounds*. 921 (2022) 166060. <https://doi.org/10.1016/j.jallcom.2022.166060>.
- [58] Li R, Wilde G, Zhang Y, Synergizing mechanical properties and damping capacities in a lightweight Al-Zn-Li-Mg-Cu alloy, *Journal of Alloys and Compounds*. 886 (2021) 161285. <https://doi.org/10.1016/j.jallcom.2021.161285>.